Meteorologische Zeitschrift, Vol. **27**, No. 1, 59–66 (published online December 19, 2017)

Lagrangian evaluation of convective shower characteristics in a convection-permitting model

Erwan Brisson[1*], Christoph Brendel[1,2], Stephan Herzog[1] and Bodo Ahrens[1]

[1]Institute for Atmospheric and Environmental Sciences, Goethe University Frankfurt, Germany.
[2]Radar group, Deutscher Wetterdienst, Offenbach, Germany.

(Manuscript received July 27, 2016; in revised form January 30, 2017; accepted March 15, 2017)

Abstract

Convection-permitting models (CPMs) have proven their usefulness in representing precipitation on a sub-daily scale. However, investigations on sub-hourly scales are still lacking, even though these are the scales for which showers exhibit the most variability. A Lagrangian approach is implemented here to evaluate the representation of showers in a CPM, using the limited-area climate model COSMO-CLM. This approach consists of tracking 5-min precipitation fields to retrieve different features of showers (e.g., temporal pattern, horizontal speed, lifetime). In total, 312 cases are simulated at a resolution of 0.01 ° over Central Germany, and among these cases, 78 are evaluated against a radar dataset. The model is able to represent most observed features for different types of convective cells. In addition, the CPM reproduced well the observed relationship between the precipitation characteristics and temperature indicating that the COSMO-CLM model is sophisticated enough to represent the climatological features of showers.

Keywords: Convection, Precipitation, Sub-hourly scale, COSMO-CLM

1 Introduction

Currently, a large gap exists between the spatiotemporal scale required by impact researchers, stakeholders, and policy makers and the scale of climate model outputs provided in the framework of climate projections (Prein et al., 2015). Filling this gap is especially challenging when focusing on precipitation, mainly because the resolution of climate models is too coarse to capture the spatial variability of precipitation required by impact models. In addition, current climate models often poorly represent precipitation on fine temporal scales (e.g., hourly) mainly as a result of deficiencies of the deep convection parametrizations. The switching-off of deep convection parametrizations is only advised for climate models with a grid-mesh fine enough for convective processes to be explicitly represented. Weisman et al. (1997) have shown that this criterion is fulfilled for a grid-mesh finer than 4 km, even if some processes involved in the development of convection are still lacking (Bryan et al., 2003). Such climate models, often referred to as convection-permitting models (CPMs), skillfully improve the representation of both the spatial and temporal variability of precipitation, thus reducing the gap between the requirements of impact researchers and model outputs.

Refining the model grid-mesh, and therefore the grid on which model output is derived, will increase the spatial variability of the precipitation field. In addition, a finer resolution allows for a more detailed description of orography in the model, which can improve the representation of precipitation in mountainous areas (Ahrens et al., 2003; Prein et al., 2013). Prein et al. (2013) and Brisson et al. (2015) have shown that the representation of the spatial variance of precipitation is also improved over flat areas with the use of CPMs compared with non-CPMs as a consequence of the improved spatial representation of showers; finer and more peaked structures result from explicitly resolving deep convection instead of using parameterizations (Brisson et al., 2015).

Explicitly resolving deep convection also improves the temporal features of convective precipitation. The timing of convective-activity peaks, occurring in the late afternoon in Western Europe, is improved (Fosser et al., 2015; Brisson et al., 2016). In addition, during convectively active periods, the representation of hourly precipitation intensities is more realistic in CPMs compared with coarser grid-mesh models (Fosser et al., 2015; Brisson et al., 2016).

While a correct representation of hourly precipitation by CPMs does not imply a correct representation of sub-hourly precipitation, hourly precipitation may be correctly represented for the wrong reasons (e.g., too long lasting precipitation events with too weak precipitation intensity). To the authors' knowledge, only idealized studies or numerical weather prediction experiments have evaluated precipitation fields on sub-hourly scales (Cohen and McCaul, 2006; Schraff et al., 2006; Singleton and Toumi, 2013), with the focus on a small number of cases, which prevents robust statistical evaluation required for the validation of climate models. The following question, therefore, remains: How well is the sub-hourly scale precipitation represented in CPMs?

*Corresponding author: Erwan Brisson, Institute for Atmospheric and Environmental Sciences, Goethe University Frankfurt, Germany, e-mail: erwan.brisson@gmail.com

The answer to this question is intrinsically related to the representation of convective precipitation in CPMs. Unlike large-scale rainfall, showers are characterized by a large temporal variability and a lifetime often shorter than an hour (Kyznarová and Novák, 2009). Realistically representing showers is, therefore, a key to providing realistic input for impact modelers who require sub-hourly scale information (e.g., urban hydrology applications). In addition, Wasko and Sharma (2015) have shown that the temporal pattern of precipitation events can be temperature dependent. A correct representation of showers, and their dependency on, for example, temperature, would be an asset for increasing our confidence in the ability of CPMs to produce realistic climate projections. For these reasons, we focus on the evaluation of shower characteristics (i.e., spatiotemporal changes of showers). Different features are specifically investigated, such as the temporal pattern, horizontal speed, or lifetime.

We adopt a Lagrangian approach to derive shower features from both an observational dataset and CPM outputs as described in Section 2. The performance of a CPM is shown in Section 3 through an evaluation of both simulated shower features and their dependency on temperature. The sensitivity of the results to the method is discussed in Section 4, while Section 5 concludes this study.

2 Methods

2.1 Observational dataset

The simulated precipitation fields are evaluated against the RZ-Radar product from Germany's National Meteorological Service (Deutscher Wetterdienst – DWD). The product used in this study covers the period 2004 to 2010, and has a 5-min temporal resolution and a spatial resolution of ~ 1 km. Further information can be found in Bartels et al. (2004) and Junghänel et al. (2015).

2.2 Simulations

All simulations investigated in this study were performed using the Consortium for Small-scale Modelling in climate mode (COSMO-CLM) model. The COSMO-CLM model is a non-hydrostatic limited-area climate model based on the COSMO model (Steppeler et al., 2003), which was designed by the Deutsche Wetterdienst (DWD) for operational weather predictions. The climate limited-area modelling (CLM) community has further developed the model to perform climate simulations (Böhm et al., 2006; Rockel et al., 2008). The two-step nesting strategy shown in Figure 1 is used to downscale ERA-Interim re-analyses (grid mesh of ~ 0.75 ° and 60 vertical levels – Simmons et al., 2007). First, a 0.22 ° simulation (CCLM022) with 200×200 grid points is performed over Europe for a 31-year period (one year is used as spin-up). This simulation is used as input to nest multiple 36-hour simulations (12 hours are used as spin-up) with a grid mesh of 0.01 ° (CCLM001) and 450 × 500 grid points. Unlike the CCLM001 simulation, the CCLM022 simulation does not explicitly resolve deep convection within the grid-scale, and hence, the deep convection scheme following the work of Tiedtke (1989) is used. CCLM001 simulations are only performed for specific cases.

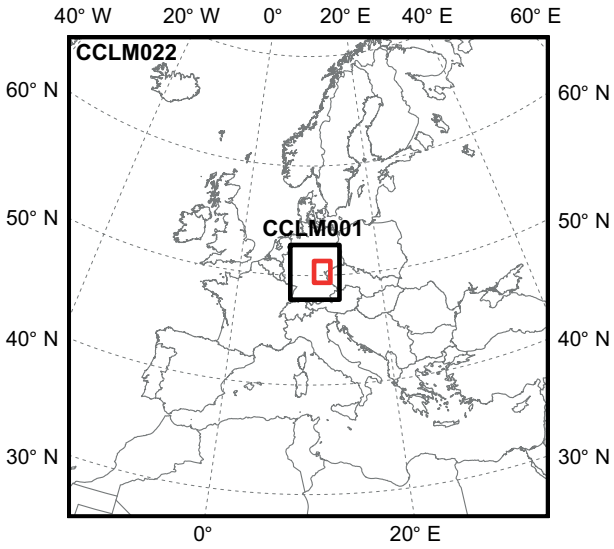

Figure 1: Map of the two COSMO-CLM simulation nests (black) and the evaluation domain (red).

Cases were selected using the method developed in Brendel et al. (2014), which is based on logistic regression models that select days with a high probability for convective activity, defined as a large number of convective cells with precipitation intensity above 8 mm/h. In addition, the identification procedure considers two types of cells independently, namely, long-lifetime cells (LLCs) which may have a significant impact over large catchments, and slowly moving cells (SMCs), which may result in the large accumulation of local precipitation. These two logistic regression models are based on predictors describing the large-scale circulation (wind speed at 850 hPa, temperature gradient at 700 hPa, etc.) or the atmospheric stability (lifted index from 0 to 3 km, vertical total index, etc.). The predictors used here are extracted from ERA-Interim data. The calibration is performed against the radar product, as described in Section 2.1, for the summer periods (here, April to September).

The method was applied for the summers from 1981 to 2010. In total, 312 days were selected: 122 of them can be characterized as days with a high probability for LLCs and 222 as days with a high probability for SMCs (22 days feature high probabilities for both LLCs and SMCs). The radar period encompasses 78 days. This method allows for selecting days with a rainfall intensity above 10 mm/h in a manner that is 6.33 times more efficient than random selection. In addition, it is also 1.31 times more efficient than selecting days based on their maximum hourly rainfall intensity over

the evaluation domain as simulated using the CCLM022 simulation.

2.3 Convective cell features

This evaluation study is based on a Lagrangian approach. An algorithm developed in Brendel et al. (2014) is used to track convective precipitation. This approach presents many advantages over a more classic grid-point evaluation approach (i.e., Eulerian approach). First, single cells can be identified and followed in time to study their temporal evolution. Second, features such as the speed or the lifetime of cells are available. Finally, the sensitivity of the analysis to the so-called "double-penalty" (Anthes, 1983) – an overestimation of model deficiencies resulting from mislocations of precipitation events – is low, although not negligible as discussed in Section 4.

A 5-min precipitation dataset is used as input for tracking convective cells. Tracks are determined in four steps:

1. A convective cell is identified by selecting neighboring grid points with a precipitation intensity greater than 20 mm/h. To avoid the selection of grid points characterized by stratiform precipitation, the identification of the convective cells is additionally conditioned to the presence of a strong gradient in precipitation intensity in the surrounding grid points.

2. The most probable location of this cell at the next timestep (indicated by gray crosses in Figure 2) is determined by assuming that the convective cell propagation is mainly driven by low-to mid-tropospheric winds, as suggested in Newton and Fankhauser (1975), Steinacker et al. (2000) or Bunkers et al. (2000). The distance and the direction of propagation is obtained from the 850 hPa, 700 hPa and 500 hPa wind fields. Besides, an area of uncertainty (indicated by circles in Figure 2) is considered around the most probable location, whose size increases with the strength of the wind speed.

3. If one convective cell (identified based on the same criteria as in step 1) is found in the area of uncertainty derived in step 2, it is associated with the convective cell found in the previous time-step. If two or more convective cells are present in the area of uncertainty, only the convective cell closest to the most probable location is chosen. Splitting and merging of the convective cells is, therefore, not considered.

4. Steps 2 and 3 are repeated until no more cells are found in step 3 (e.g., as at time-step t4 in Figure 2).

The tracking algorithm is applied to the radar dataset and the model output independently. For the radar dataset, the wind fields required to derive the most probable locations, as well as their associated uncertainties, are extracted from the NCEP reanalysis (Kalnay et al., 1996).

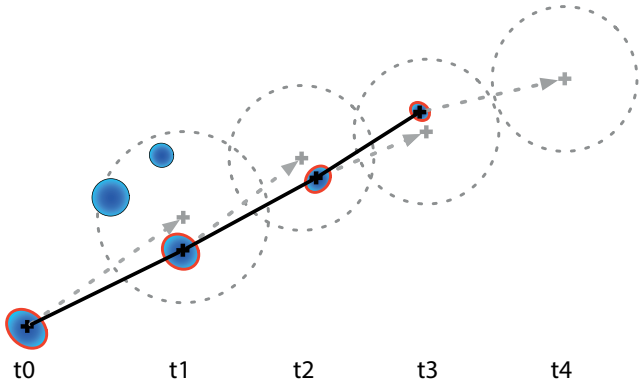

Figure 2: Illustration of the tracking algorithm for an idealized case for five timesteps. The blue shapes indicate precipitation patterns that are identified as convective cells at a specific timestep. The red contour shows the precipitation patterns corresponding to one single cell according to the tracking algorithm. The gray dashed arrows show the ideal propagation of the cell under investigation according to the wind fields, while the gray crosses and circles indicate the most probable cell locations and their uncertainties, respectively.

For the model output, this information is obtained using the CCLM022 wind fields.

For each cell, the 5-min precipitation accumulations, the cell lifetime and the cell horizontal speed are extracted. To study the evolution of showers with different lifetimes, the quantity

$$P_t\prime = \frac{P_t}{\bar{P}} \tag{2.1}$$

is introduced, where P_t is the precipitation intensity at time-step t and $\bar{P}$ is the mean precipitation intensity of the cell. The mean of $P\prime$ is, thus, equal to 1.

Similar to Goudenhoofdt and Delobbe (2013), cells with a lifetime shorter than 15 min are discarded. In addition, cells starting or ending at the border of the evaluation domain are also discarded. Finally, a specific post-processing is applied to the track derived from the radar dataset. Grid points with unrealistically high signals are referred to as clutter-pixels. Only tracks including at least one grid point that is not a clutter-pixel are considered. These steps filter out falsely identified tracks resulting from artifacts such as radar beam reflections from obstacles, including those with varying reflections, such as wind turbines.

The probability density function (PDF) of modeled shower features are evaluated against radar-detected showers using the Perkins Skill Score (PSS – Perkins et al., 2007), which measures the common area between two PDFs by calculating their cumulative minimum for each group of binned values,

$$PSS = \sum_{i=1}^{n} \min(Z_{\text{model}}(i), Z_{\text{radar}}(i)), \tag{2.2}$$

where i is the bin index, n is the total number of bins, and $Z_{\text{model}}(i)$ and $Z_{\text{radar}}(i)$ are the model- and radar-

probabilities masses respectively. Two PDFs are identical when the PSS is equal to 1. In addition, Perkins et al. (2007) suggests that two PDFs differ significantly from each other when their PSS is lower than ~ 0.7. This calculation is also applied for the evaluation of $P\prime$.

3 Results

Figure 3 shows the averaged temporal evolution of observed and modeled precipitating convective cells. Observed $P\prime$ increases strongly in the first 15 % of the cell's lifetime, reaching its maximum at 25 % of the cell's lifetime and decreasing from that point on. The maximum $P\prime$ reaches 1.06. The amplitude of the average cell, which is the difference between the maximum and minimum $P\prime$, is about 0.2.

The model simulations follow the observed temporal pattern closely and explain more than 98 % of the observed temporal variance. The overlap between the observed and the model temporal pattern is 99.6 %. The maximum value and the amplitude of $P\prime$ show minor biases with average values of 1.06 and 0.22 of the cell-mean 5-min accumulations, respectively. However, $P\prime$ for the first 10 % of the precipitating cell lifetime is underestimated by up to 3 %, and the occurrence of the maximum $P\prime$ is slightly delayed (4 % of the cell lifetime – 1.5 min for a typical cell lifetime).

These latter two biases partly arise from less frequent short-lifetime events (i.e., with cell lifetimes < 30 min) in the simulations compared with radar observations (as shown later). Short-lifetime events represent more than 43 % of all events and, therefore, significantly influence the average temporal pattern of the convective events shown in Figure 3. The very short-lifetime events (i.e., with cell lifetimes of 15 min), which are characterized by lower precipitation temporal evolution (i.e., flattened line), are detected 34 % more often in the radar dataset than in the model simulations. The source of this bias is discussed in Section 4.

The bias of $P\prime$ maximum occurrence is reduced with increasing cell lifetimes (Figure 4(a)). The delay between the model and the observation is 10 % for short-lifetime events (i.e., with cell lifetimes < 30 min) and 1 % for long events (i.e., with cell lifetimes > 90 min). Although the highest values of $P\prime$ are slightly underestimated by the CPM, the simulations capture the increase in temporal variability (higher maximum values) with increased lifetimes. In addition, the probability of occurrence of events longer than 30 min in the model is close to the one observed in the radar dataset (Figure 5).

$P\prime$ shows the highest variability at the beginning and the end of shower tracks (Figure 4(b)). While the model reproduces the temporal pattern of the $P\prime$ standard deviation well, it underestimates the standard deviation by ~ 20 %. This underestimation is larger for very short-lifetime events (up to 30 %) and remains below 15 % for longer events (Figure 4(b)). The selection procedure, described in Section 2.2, considers two different types

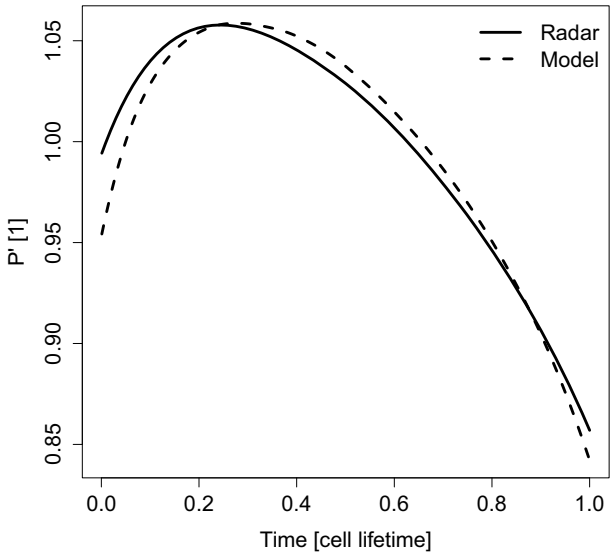

Figure 3: Averaged temporal evolution of $P\prime$ for all convective cells according to the radar (solid line) and the model (dashed line) results.

Table 1: The number of all convective cells, cells occuring during days with a high probability for long lifetime cells (LLC-day cells) and cells occuring during days with a high probability for slowly moving cells (SMC-day cells) detected in the radar dataset and the model output.

Dataset	All cells	LLC-day cells	SMC-day cells
Radar	40741	15754	24987
Model	38964	16462	22502

of cells, namely, the LLCs and the SMCs. Below, the cells are classified based on whether they occur during a day with a high probability for the occurrence of LLCs (LLC-day cells) or SMCs (SMC-day cells). The LLC-day cells occur more often than the SMC-day cells, with 61 % and 39 % of all cells, respectively. The model is able to reproduce this distribution with a bias smaller than 4 % (Table 1). As shown in Figs. 5 and 6, the duration and horizontal speed distribution of the LLC-day cells and SMC-day cells differ significantly from each other. The Perkins skill scores (PSSs) between the LLC-day cells and SMC-day cells reached ~ 0.67 and ~ 0.25 for the duration and the horizontal speed, respectively, and thus indicate significant differences following Perkins et al. (2007).

The LLC-day cells feature a higher probability for long lasting events (> 1 hour) and a lower probability for short-lifetime events (< 1 hour) than the SMC-day cells. This feature is reproduced well by the model, with PSSs of 0.96 and 0.90 for the LLC-day cells and SMC-day cells, respectively.

As shown in Figure 6, the model produces close-to-observed horizontal speed distributions for each of the cells types (i.e., LLC-day cells and SMC-day cells). The PSS notably reached 0.86 for the LLC-day cells and 0.89 for the SMC-day cells. Surprisingly, the PSS was higher (0.96) when considering all events, and resulted

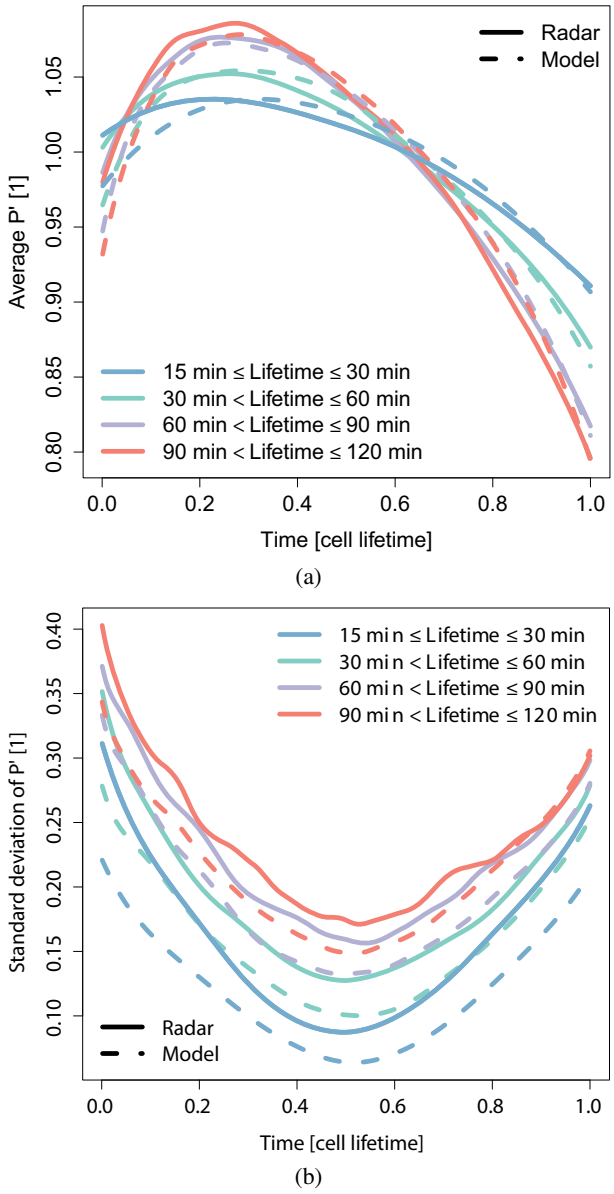

Figure 4: Averages (a) and standard deviations (b) of $P\prime$ for convective cells with different lifetimes (shown in different colors). Averages and standard deviations derived from the radar are shown with solid lines, while those derived from the model are shown with dashed lines.

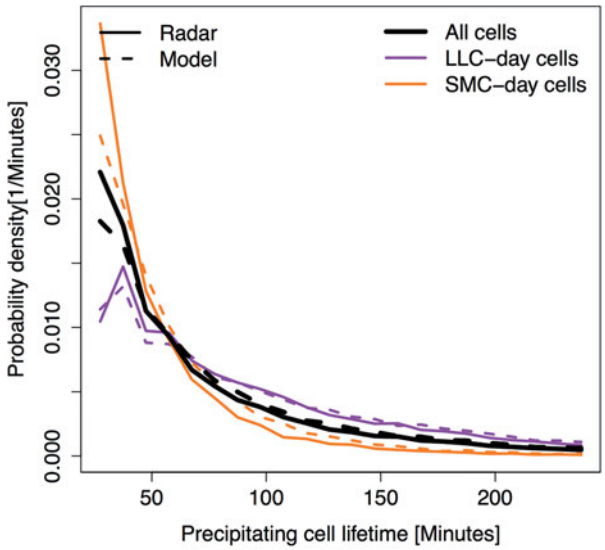

Figure 5: Cell lifetime probability density for all cells (in black) and for convective cells occuring during days with a high probability for long lifetime cells (LLC-day cells – in purple) and cells occuring during days with a high probability for slowly moving cells (SMC-day cells – in orange). Probabilities derived from the radar are shown as solid lines, while those derived from the model are shown as dashed lines.

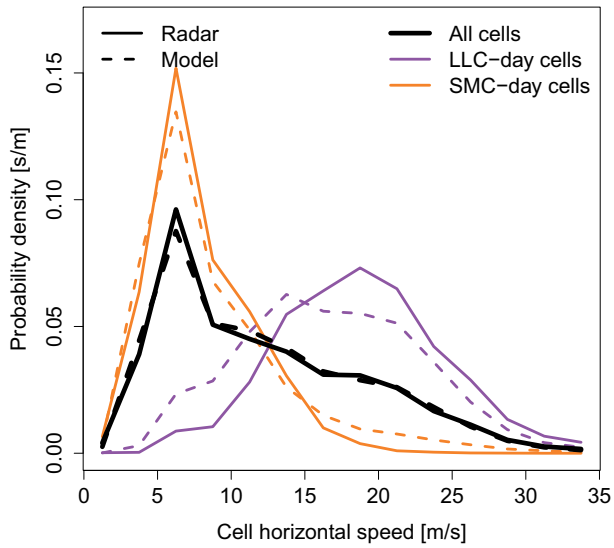

Figure 6: Cell horizontal speed probability density for all cells (in black) and for convective cells occuring during days with a high probability for long lifetime cells (LLC-day cells – in purple) and cells occuring during days with a high probability for slowly moving cells (SMC-day cells – in orange). Probabilities derived from the radar are shown as solid lines, while those derived from the model are shown as dashed lines.

from compensation of biases between the two types of cells. The occurrence probability of the slowest SMC-day cells (LLC-day cells) – <15 m/s – were underestimated (overestimated), while the occurrence probability of SMC-day cells (LLC-day cells) faster than 15 m/s were overestimated (underestimated).

The shower temporal pattern on temperature was investigated by Wasko and Sharma (2015), who found that at higher temperatures, the temporal pattern of precipitation becomes less uniform (i.e., the highest (lowest) $P\prime(t)$ become higher (lower)). The linear regression between the mean daily 2 m-temperature (provided by the CPMs) and the daily average of the maximum $P\prime$ for each convective cell shows that such a temperature-scaling of the temporal precipitation pattern is also observed over Central Germany. The scaling is of similar amplitude in both the observation with a coefficient of 0.37 %/K (significant at the 5 % level) and in the model with a coefficient of 0.46 %/K (significant at the 1 % level) for the CPM.

4 Discussion

While the COSMO-CLM simulations are able to capture most of the characteristics of showers, very short-lifetime events, especially those occuring during SMC-days, are severely underestimated in the model for the following possible reasons:

1. The model is unable to reproduce the very short-lifetime events.

2. Not all artifacts of the radar dataset, such as clutter, have been successfully filtered out (as described in Section 2.3). Some remaining artifacts may therefore be considered as very short-lifetime events in the analysis.

3. The wind fields used to determine the probable location of convective cells (step 2 in Section 2.3) could be biased, which may cause the tracking algorithm to fail in retrieving the full path of the convective cells and, therefore, result in a subdivision of long cell tracks into multiple short-lifetime ones. The low spatiotemporal resolution of the NCEP dataset may explain a high occurrence of subdivisions in the radar datasets. When applying the tracking algorithm to model data, such subdivisions are less likely to occur. Indeed, first, the wind fields from the CCLM022 simulation, used to track convective cells in the model are characterized by a high spatiotemporal resolution. Second, even if misrepresented, these wind fields are part of the forcing of the CCLM001 and are, therefore, highly accurate in inferring the direction of modeled convective cells.

Although it is not possible to invalidate (1) and (2), some clues point to the important role of (3) in the underestimation of short-lifetime events in the CPM outputs compared with the radar dataset. First, the model underestimates the total number of all cells – including those with a lifetime shorter than 15 min – by 25 %, while the sum of showers with all lifetimes is overestimated by 10 %. Figure 5 shows that the underestimation of SMC-day cells with lifetimes shorter than 50 min are compensated by cells with longer lifetimes. Second, the ratio of the short-lifetime event to the total number of events in the radar dataset is significantly correlated (i.e., a Pearson coefficient of 0.82, which is significant at the 1 % level) to the standard deviation of the wind direction (the standard deviation is derived using the Yamartino (1984) method). This indicates that on days characterized by large changes in the wind direction, changes not necessarily appearing in the NCEP re-analysis, results in the proportion of short-lifetime showers higher than on days with constant wind directions. A possible explanation for this result is the higher chance for subdividing long tracks into smaller ones on days with large and recurring changes in the wind direction. Finally, (3) is supported by visualizing the radar dataset (a qualitative approach).

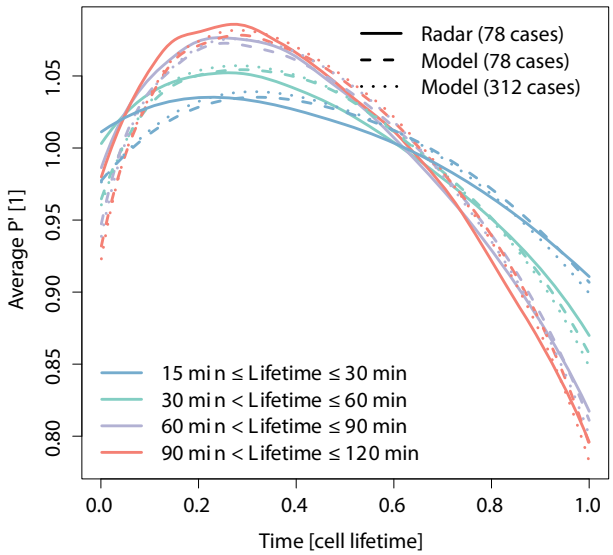

Figure 7: Averages of $P\prime$ for convective cells with different lifetimes (shown in different colors) for 78 cases (radar – solid line, model – dashed line) and for 312 cases (model – dotted line).

The simulation period with available radar data limits the evaluation here to 78 cases. As shown in Figure 7 for the temporal pattern, the features of showers shown in Section 3 are similar to those derived by using all 312 simulated cases. In addition, calibrating the linear regression model established in Section 3 with all cases, instead of only 78 cases, results in a similar coefficient (0.30 %/K, which is significant at the 1 % level). However, a relation between temperature and other shower features, which cannot be detected – at least not at a significant level – with 78 cases, may be established when using 312 cases. The time-period for which radar data is available may, therefore, limit the evaluation of the possible relationships between temperature and the different features of showers.

5 Conclusions

A Lagrangian approach is applied here to a radar dataset and CPM outputs. By evaluating different features of showers, this approach allowed for improving our understanding of CPM performance at time-scales that are rarely explored (i.e., a scale of 5 min). Information on such time-scales are particularly useful for climate impact modelers (e.g., urban hydrologist).

The results of this study show that for events with a cell lifetime greater than 30 min, shower features (i.e., the number, lifetime, temporal evolution, and horizontal speed) are reproduced well by the COSMO-CLM at the convection-permitting scale. For very short-lifetime events (i.e., with cell lifetimes < 30 min), uncertainties, probably related to the methodology, are too high for any conclusions to be drawn.

In addition, the CPM is able to reproduce the observed increase of the maximum precipitation in the temporal pattern of precipitating convective cells with

temperature, which provides further confidence that the CPM may be applied to a warmer climate in the context of climate projections.

This study, therefore, tends to support the hypothesis that the representation of the physics and the numerics in CPMs is sophisticated enough to reproduce the present-day climatology of convective precipitation. However, convection impacts on other fields, such as radiative forcing or different convective hazards (e.g., lightning, hail, wind gusts), are not evaluated here. Depending on the availability of observations, the method developed here may also be applied to such fields.

Acknowledgments

Calculations on the LOEWE-CSC high-performance computer of the Frankfurt University were conducted for this research. Bodo Ahrens acknowledges support from Senckenberg BiK-F. The NCEP Reanalysis data was provided by the NOAA/OAR/ESRL PSD, Boulder, Colorado, USA, from their website at http://www.esrl.noaa.gov/psd/. The RZ-Radar product was provided by the German National Meteorological Service (Deutscher Wetterdienst – DWD).

References

Ahrens, B., K. Jasper, J. Gurtz, 2003: On ALADIN precipitation modeling and validation in an Alpine watershed. – Ann. Geophys. **21**, 627–637, DOI: 10.5194/angeo-21-627-2003.

Anthes, R.A., 1983: Regional Models of the Atmosphere in Middle Latitudes. – Monthly Weather Review **111**, 1306–1335, DOI: 10.1175/1520-0493(1983)111<1306:RMOTAI>2.0.CO;2.

Bartels, H., E. Weigl, T. Reich, P. Lang, A. Wagner, O. Kohler, N. Gerlach, MeteoSolutions GmbH, 2004: Projekt RADOLAN – Routineverfahren zur Online-Aneichung der Radarniederschlagsdaten mit Hilfe von automatischen Bodenniederschlagsstationen (Ombrometer), 111 pp.

Böhm, U., M. Kücken, W. Ahrens, A. Block, D. Hauffe, K. Keuler, B. Rockel, A. Will, 2006: CLM – The Climate Version of LM: Brief Description and Long-Term Applications. – COSMO Newsletter **6**, 225–235.

Brendel, C., E. Brisson, F. Heyner, E. Weigl, B. Ahrens, 2014: Bestimmung des atmosphärischen Konvektionspotentials über Thüringen. – Berichte des Deutschen Wetterdienstes **244**, 72 pp.

Brisson, E., M. Demuzere, N.P.M.V. Lipzig, 2015: Modelling strategies for performing convection-permitting climate simulations. – Meteorol. Z. **25**, 149–163, DOI: 10.1127/metz/2015/0598.

Brisson, E., K. Van Weverberg, M. Demuzere, A. Devis, S. Saeed, M. Stengel, van N.P. M. Lipzig, 2016: How well can a convection-permitting climate model reproduce decadal statistics of precipitation, temperature and cloud characteristics?. – Climate Dynam. **47**, 3043–3061, DOI: 10.1007/s00382-016-3012-z.

Bryan, G.H., J.C. Wyngaard, J.M. Fritsch, 2003: Resolution Requirements for the Simulation of Deep Moist Convection. – Mon. Wea. Rev. **131**, 2394–2416, DOI: 10.1175/1520-0493(2003)131<2394:RRFTSO>2.0.CO;2.

Bunkers, M.J., B.A. Klimowski, J.W. Zeitler, R.L. Thompson, M.L. Weisman, 2000: Predicting Supercell Motion Using a New Hodograph Technique. – Wea. Forecast. **15**, 61–79, DOI: 10.1175/1520-0434(2000)015<0061:PSMUAN>2.0.CO;2.

Cohen, C., E.W. McCaul, 2006: The Sensitivity of Simulated Convective Storms to Variations in Prescribed Single-Moment Microphysics Parameters that Describe Particle Distributions, Sizes, and Numbers. – Mon. Wea. Rev. **134**, 2547–2565, DOI: 10.1175/MWR3195.1.

Fosser, G., S. Khodayar, P. Berg, 2015: Benefit of convection permitting climate model simulations in the representation of convective precipitation. – Climate Dynam. **44**, 45–60, DOI: 10.1007/s00382-014-2242-1.

Goudenhoofdt, E., L. Delobbe, 2013: Statistical Characteristics of Convective Storms in Belgium Derived from Volumetric Weather Radar Observations. – J. Appl. Meteor. Climatol. **52**, 918–934, DOI: 10.1175/JAMC-D-12-079.1.

Junghänel, T., C. Brendel, T. Winterrath, A. Walter, 2015: Towards a radar- and observation-based hail climatology for Germany. – Meteorol. Z. **25**, 435–445, DOI: 10.1127/metz/2016/0734.

Kalnay, E., M. Kanamitsu, R. Kistler, W. Collins, D. Deaven, L. Gandin, M. Iredell, S. Saha, G. White, J. Woollen, Y. Zhu, A. Leetmaa, R. Reynolds, M. Chelliah, W. Ebisuzaki, W. Higgins, J. Janowiak, K.C. Mo, C. Ropelewski, J. Wang, R. Jenne, D. Joseph, 1996: The NCEP/NCAR 40-Year Reanalysis Project. – Bull. Amer. Meteor. Soc. **77**, 437–471, DOI: 10.1175/1520-0477(1996)077<0437:TNYRP>2.0.CO;2.

Kyznarová, H., P. Novák, 2009: CELLTRACK – Convective cell tracking algorithm and its use for deriving life cycle characteristics. – Atmos. Res. **93**, 317–327, DOI: 10.1016/j.atmosres.2008.09.019.

Newton, C.W., J.C. Fankhauser, 1975: Movement and propagation of multicellular convective storms. – Pure Appl. Geophys. **113**, 747–764, DOI: 10.1007/BF01592957.

Perkins, S.E., A.J. Pitman, N.J. Holbrook, J. McAneney, 2007: Evaluation of the AR4 Climate Models' Simulated Daily Maximum Temperature, Minimum Temperature, and Precipitation over Australia Using Probability Density Functions. – J. Climate **20**, 4356–4376, DOI: 10.1175/JCLI4253.1.

Prein, A.F., G.J. Holland, R.M. Rasmussen, J. Done, K. Ikeda, M.P. Clark, C.H. Liu, 2013: Importance of Regional Climate Model Grid Spacing for the Simulation of Heavy Precipitation in the Colorado Headwaters. – J. Climate **26**, 4848–4857, DOI: 10.1175/JCLI-D-12-00727.1.

Prein, A.F., W. Langhans, G. Fosser, A. Ferrone, N. Ban, K. Goergen, M. Keller, M. Tölle, O. Gutjahr, F. Feser, E. Brisson, S. Kollet, J. Schmidli, N.P.M. Van Lipzig, R. Leung, 2015: A review on regional convection-permitting climate modeling: Demonstrations, prospects, and challenges. – Rev. Geophys. **53**, 323–361, DOI: 10.1002/2014RG000475.

Rockel, B., A. Will, A. Hense, 2008: The Regional Climate Model COSMO-CLM (CCLM). – Meteorol. Z. **17**, 347–348, DOI: 10.1127/0941-2948/2008/0309.

Schraff, C., K. Stephan, S. Klink, 2006: Revised Latent Heat Nudging to cope with Prognostic Precipitation. – COSMO Technical report **6**.

Simmons, A.J., S. Uppala, D. Dee, S. Kobayashi, 2007: ERA-interim: new ECMWF reanalysis products from 1989 onwards. – ECMWF Newsletter **110**, 25–35.

Singleton, A., R. Toumi, 2013: Super-Clausius-Clapeyron scaling of rainfall in a model squall line. – Quart. J. Roy. Meteor. Soc. **139**, 334–339, DOI: 10.1002/qj.1919.

Steinacker, R., M. Dorninger, F. Wolfelmaier, T. Krennert, 2000: Automatic Tracking of Convective Cells and Cell Complexes from Lightning and Radar Data. – Meteor. Atmos. Phys. **72**, 101–110, DOI: 10.1007/s007030050009.

Steppeler, J., G. Doms, U. Schättler, H.W. Bitzer, A. Gassmann, U. Damrath, G. Gregoric, 2003: Meso-gamma scale forecasts using the nonhydrostatic model LM. – Meteor. Atmos. Phys. **82**, 75–96, DOI: 10.1007/s00703-001-0592-9.

Tiedtke, M., 1989: A Comprehensive Mass Flux Scheme for Cumulus Parameterization in Large-Scale Models. – Mon. Wea. Rev. **117**, 1779–1800, DOI: 10.1175/1520-0493(1989)117<1779:ACMFSF>2.0.CO;2.

Wasko, C., A. Sharma, 2015: Steeper temporal distribution of rain intensity at higher temperatures within Australian storms. – Nature Geoscience **8**, 527–530, DOI: 10.1038/ngeo2456.

Weisman, M.L., W.C. Skamarock, J.B. Klemp, 1997: The Resolution Dependence of Explicitly Modeled Convective Systems. – Mon. Wea. Rev. **125**, 527–548, DOI: 10.1175/1520-0493(1997)125<0527:TRDOEM>2.0.CO;2.

Yamartino, R.J., 1984: A Comparison of Several "Single-Pass" Estimators of the Standard Deviation of Wind Direction. – J. Climate Appl. Meteor. **23**, 1362–1366, DOI: 10.1175/1520-0450(1984)023<1362:ACOSPE>2.0.CO;2.